NATIONAL ADVISORY COMMITTEE FOR AERONAUTICS

TECHNICAL NOTE 2388

AXISYMMETRIC SUPERSONIC FLOW IN ROTATING IMPELLERS

By Arthur W. Goldstein

Lewis Flight Propulsion Laboratory
Cleveland, Ohio

Washington
June 1951

NATIONAL ADVISORY COMMITTEE FOR AERONAUTICS

TECHNICAL NOTE 2388

AXISYMMETRIC SUPERSONIC FLOW IN ROTATING IMPELLERS

By Arthur W. Goldstein

SUMMARY

General equations are developed for isentropic, frictionless, axisymmetric flow in rotating impellers with blade thickness taken into account and with blade forces eliminated in favor of the blade-surface function. It is shown that the total energy of the gas relative to the rotating coordinate system is dependent on the stream function only, and that, if the flow upstream of the impeller is vortex-free, a velocity-potential function of only the radial and axial distances exists in the impeller.

The characteristic equations for supersonic flow are developed and used to investigate flows in several configurations in order to ascertain the effect of variations of the boundary conditions on the internal flow and the work input. Conditions varied are prerotation of the gas, blade turning rate, gas velocity at the blade tips, blade thickness, and sweep of the leading edge.

INTRODUCTION

No method of practical importance has been described in the literature for computing the flow in the three-dimensional region between the blades of the supersonic compressor. This deficiency in design technique has been partly met by using two-dimensional theory to compute the variations of the relative flow from blade to blade, by assuming no radial flow components, and by neglecting spanwise variations. This procedure is probably satisfactory for designs with ratio of blade-root radius to blade-tip radius close to unity, and cylindrical hub and casing shape. When this ratio is small, the spanwise variations are significant. A method is described herein, which was devised at the NACA Lewis laboratory, for computing the magnitude of these variations, when blade-to-blade variations are neglected, by assuming a large number of blades in the impeller and dealing with the circumferential average flow. This technique, when combined with estimates of blade-to-blade variations, is useful for designs with closely spaced blades.

The usefulness of this approach may possibly be extended to supersonic flow in a manner analogous to the method described in reference 1 for subsonic flow; the axisymmetric solution is first found and then used as a base for computing the blade-to-blade variations. The particular method used in the blade-to-blade calculation of reference 1 is series expansion, which is not applicable to supersonic flows because of the existence of solutions with discontinuous derivatives.

In reference 2, the equations for internal flow with zero blade thickness are translated into the characteristic equations for the derivatives of the stream function, and it is shown there that the equations are hyperbolic if the relative velocity is supersonic, provided the ratio of the tangential to the axial velocity is a given field function. (This condition includes the special class of blades containing radii from the axis of rotation). If the tangential velocity is prescribed, then the meridional velocity component is the decisive factor in determining whether the equations are hyperbolic.

The present report treats the velocity components directly after the manner of reference 3 for arbitrary preassigned blade shapes. The design problem is solved by finding the hub shape that will give a prescribed velocity distribution along the casing (or any other selected stream surface). In the course of the solution, the tangentially averaged flow is completely determined in the interior of the impeller.

The purpose of this paper, in addition to describing the method in a mathematical outline, is to examine the performance of the technique in computed examples and to find if any peculiarities in the flow arise from the boundary conditions imposed, and to develop a background of experience for the design of impellers of the type considered by examination of the effect of systematic variations of impeller design parameters on the internal flow. The parameters varied are inlet prerotation, blade turning rate, gas velocity distribution at the casing, blade thickness, and sweep of the blade leading edge.

Approximately 160 hours of computing is required to work out about 100 points for each of the impellers. This time can be reduced by application of the punched-card computing technique to part of the procedure.

DEVELOPMENT OF EQUATIONS FOR AXIALLY SYMMETRIC FLOW

Equations describing the fluid flow are developed in convenient form by use of the equations of motion and continuity, the conditions of axial symmetry, and isentropic state changes. The uniformly distributed blade forces, which are inconvenient in calculations, are

eliminated from the equations by substituting the blade surface function, so that the condition of integrability is automatically satisfied.

Equation of Continuity

The continuity equation for steady flow is

$$\nabla \cdot (\rho W) = 0$$

(Symbols are defined in the appendix.) If axial symmetry is assumed, the equivalent in cylindrical coordinates is

$$\frac{\partial}{\partial r}(\rho v r) + \frac{\partial}{\partial z}(\rho w r) = 0$$

The presence of blades serves to modify these equations if the space filled by the blades is taken into account. If the impeller contains N blades with thickness t measured in the direction of rotation, the ratio of volume available for fluid flow to the actual volume of any space element approaches (in the limit as the number of blades increases indefinitely with Nt fixed)

$$\frac{A}{r} = 1 - \frac{Nt}{2\pi r}$$

The continuity equation is therefore obtained by reducing the specific-mass-flow terms ρv and ρw by the ratio A/r to account for the area reduction:

$$\frac{\partial}{\partial r}(\rho v A) + \frac{\partial}{\partial z}(\rho w A) = 0 \qquad (1)$$

Because none of the scalar quantities is a function of θ, equation (1) implies the existence of a stream function $\psi(r,z)$ such that

$$\left.\begin{aligned} \psi_r &= \rho w A \\ \psi_z &= -\rho v A \\ \psi_\theta &= 0 \end{aligned}\right\} \qquad (2)$$

(subscripts indicate partial derivatives) or

$$\nabla\psi = \rho A j \times V = \rho A j \times W \tag{2a}$$

Equation of Motion

Substitution of energy for pressure. - The equation of motion for steady, nonviscous, isentropic flow in terms of the relative velocity is

$$\nabla \frac{W^2}{2} - W \times \nabla \times W + \frac{1}{\rho}\nabla p = \omega^2 R + 2W \times \Omega + F$$

where $\omega^2 R$ is the centrifugal force and $2W \times \Omega$ the Coriolis force. For isentropic conditions, the substitution

$$\frac{1}{\rho}\nabla p = \nabla h$$

may be made, so that the equation is then

$$\nabla\left(h + \frac{W^2}{2} - \frac{\omega^2 r^2}{2}\right) = W \times (\nabla \times W + 2\Omega) + F = W \times \nabla \times V + F \tag{3}$$

The quantity

$$E \equiv h + \frac{W^2}{2} - \frac{\omega^2 r^2}{2} = h + \frac{V^2}{2} - \omega r(u + \omega r) \tag{4}$$

is a measure of the total energy of the gas particles in the relative system of coordinates and remains constant (as will be shown for frictionless flow) for any particle; energy is interchanged among the forms of enthalpy, kinetic energy, and potential energy ($-\omega^2 r^2/2$) resulting from the centrifugal-force field. In reference 2, E is shown to be constant for any particle for frictionless flow and no heat transfer, with a finite number of blades in the impeller.

In order to show that E is constant for any particle in axially symmetric flow, the direction of the field force is first identified. If the blades are considered to increase indefinitely in number and to retain their camber-line shape, the forces exerted by the blades are merely the pressure forces exerted normal to the blade surfaces, which in the limit approach uniformly distributed forces in the body of the fluid. The relative flow lines are always contained in one of the family of blade surfaces, so that the field or blade forces must be normal to the velocity. If the scalar product of equation (3) is taken with the relative velocity, the result is then

$$W \cdot \nabla E = 0$$

which indicates that E does not change along any flow line.

Elimination of blade force. - The blade force can be eliminated from the equation of motion if the equation for the blade surfaces is assumed known. The force may then be evaluated after the velocity components are known.

Under the condition of axial symmetry, the equation for the family of blade surfaces

$$\alpha(r, \theta, z) = \text{constant}$$

may be simplified. If the constant is changed, there is a shift from one blade to another. Because of axial symmetry, this shift is equivalent to rotating the original blade by a fixed angle. Therefore, the equation for the surfaces can be put into the form

$$\alpha = \theta + f(r,z) \tag{5}$$

Because the relative-velocity flow lines are contained in the blade surfaces, W is normal to $\nabla\alpha$ as well as normal to $\nabla\psi$. Therefore, the relation among the three vectors can be shown to be

$$W = \frac{r}{\rho A}\nabla\psi \times \nabla\alpha \tag{6}$$

From the condition of axial symmetry,

$$\frac{\partial E}{\partial \theta} = rj \cdot \nabla E = 0$$

Because both ∇E and $\nabla\psi$ are normal to j and W, they must be parallel, and consequently E is known to be a function of ψ only (reference 4); that is,

$$\left.\begin{aligned} E &= E(\psi) \\ \nabla E &= \nabla\psi \frac{dE}{d\psi} \end{aligned}\right\} \tag{7}$$

Insertion of equations (4), (6), and (7) into equation (3) yields (without resolution of the term $\nabla \times V$)

$$\frac{dE}{d\psi}\nabla\psi = \left(\frac{r}{\rho A}\nabla\psi \cdot \nabla \times V\right)\nabla\alpha - \left(\frac{r}{\rho A}\nabla\alpha \cdot \nabla \times V\right)\nabla\psi + F$$

The blade pressure forces F are normal to the blades and therefore parallel to $\nabla\alpha$; this relation thus includes only two nonparallel vectors $\nabla\alpha$ and $\nabla\psi$, so that the components must separately satisfy the relations

$$F = -\left(\frac{r}{\rho A}\nabla\psi \cdot \nabla \times V\right)\nabla\alpha = -(rj \cdot W \times \nabla \times V)\nabla\alpha \tag{8}$$

and

$$\frac{dE}{d\psi} = -\frac{r}{\rho A}\nabla\alpha \cdot \nabla \times V \tag{9}$$

Special conditions. - Two special conditions of technical importance are considered: In high-speed machines, blades with radial elements are desirable in order to eliminate bending loads resulting from centrifugal forces. Another frequently occurring circumstance is that of zero vorticity upstream of the impeller.

For blades with radial elements, the vector i lies in the blade surface and therefore

$$i \cdot \nabla\alpha = f_r = 0$$

Therefore f is a function of z alone. From equation (6),

$$0 = W \cdot \nabla\alpha = \frac{u}{r} + vf_r + wf_z \tag{10}$$

so that for radial blade elements

$$u = -w\,r\,\frac{df}{dz} \tag{10a}$$

This relation provides considerable simplification of the equations developed later for solving the flow problem.

For vortex-free flow upstream of the impeller, equation (3) is reduced for conditions there by setting $\Omega = F = \nabla \times V = 0$ and substituting V for W to get

$$\nabla\left(h + \frac{V^2}{2}\right) = 0$$

or

$$h + \frac{V^2}{2} = \text{constant}$$

Also, zero vorticity gives, for axial symmetry,

$$0 = \nabla \times V = - i \frac{\partial}{\partial z} (u + \omega r) + j \left(\frac{\partial v}{\partial z} - \frac{\partial w}{\partial r} \right) + \frac{k}{r} \frac{\partial}{\partial r} (ur + \omega r^2)$$

From the first and last terms and axial symmetry,

$$ur + \omega r^2 = \text{constant}$$

Then the value of the total energy E relative to the impeller is

$$E = h + \frac{W^2}{2} - \frac{\omega^2 r^2}{2} = h + \frac{V^2}{2} - \omega(ru + \omega r^2)$$

which is constant upstream of the impeller. Then by equation (7) E remains constant in the impeller, so that the equation of motion (9) becomes

$$\nabla \alpha \cdot \nabla \times V = 0 \tag{11}$$

If the system of coordinates used is r, z, and α for expressing equation (11), there results (reference 4)

$$\frac{\partial}{\partial z} (rV \cdot \nabla \alpha \times k) \Big|_{r,\alpha} = \frac{\partial}{\partial r} (rV \cdot i \times \nabla \alpha) \Big|_{z,\alpha}$$

The subscripts indicate which variables are held constant. This equation and the fact that the quantities in parentheses are functions of r and z only establish the existence of a potential function of r and z only $(\Phi(r,z))$ such that

$$\frac{\partial \Phi}{\partial r} \Big|_{z,\alpha} = rV \cdot \nabla \alpha \times k$$

$$\frac{\partial \Phi}{\partial z} \Big|_{r,\alpha} = rV \cdot i \times \nabla \alpha$$

$$\frac{\partial \Phi}{\partial \alpha} \Big|_{r,z} = 0$$

The last relation indicates that with r and z constant, Φ is constant, and this is true regardless of the third independent variable, which may be taken as θ. The three equations for Φ are then put into vector form:

$$\nabla \Phi = i(rV \cdot \nabla\alpha \times k) + k(rV \cdot i \times \nabla\alpha) \tag{12}$$

The absolute velocity may then be shown to be

$$V = \nabla\Phi + r(u + \omega r)\nabla\alpha \tag{13}$$

and from

$$V \cdot \nabla\alpha = W \cdot \nabla\alpha + \omega r j \cdot \nabla\alpha = \omega$$

equation (13) gives for the moment of momentum μ,

$$\mu \equiv r(u + \omega r) = \frac{\omega - \nabla\Phi \cdot \nabla\alpha}{(\nabla\alpha)^2} \tag{14}$$

so that

$$V = \nabla\Phi + \frac{(\omega - \nabla\alpha \cdot \nabla\Phi)}{(\nabla\alpha)^2}\nabla\alpha \tag{13a}$$

The potential Φ can be used as an alternative to the stream function in solving for the flow. Equation (13) indicates that the projection of $\nabla\Phi$ on the blade surface is equal to the projection of the absolute velocity on the blade surface. The equation for ψ and that for Φ are obtained in the following manner: The velocity V is eliminated from equation (9) by means of equation (6) and there is obtained

$$\nabla\alpha \cdot \nabla \times \left(\frac{r}{\rho A}\nabla\psi \times \nabla\alpha\right) + 2\omega f_z = -\frac{\rho A}{r}\frac{dE}{d\psi}$$

which is also applicable in the general case with nonzero vorticity upstream of the impeller.

In order to obtain an equation for Φ, equation (13a) is substituted into equation (2a):

$$\nabla\psi = \rho Ar\nabla\theta \times V = \rho Ar\nabla\theta \times \nabla\Phi + \rho A\mu r\nabla\theta \times \nabla\alpha$$

Then

$$0 = \nabla \times \nabla\psi = \nabla \times \left[\rho Ar\nabla\theta \times (\nabla\Phi + \mu\nabla\alpha)\right]$$

Although obtaining a solution in terms of ψ is feasible whether $dE/d\psi$ is zero or not, when $dE/d\psi = 0$, Φ may prove more convenient. In regions where W^2/a^2 is nearly 1.0, because $|W|$ is a double-valued function of the stream-function derivative $\rho|W|$, it will be uncertain whether the flow is subsonic or supersonic. A solution obtained from a network would require a very fine spacing in regions where $|W| \approx a$.

General Equations in Cylindrical Coordinates

In general, where $f_r \neq 0$ and $dE/d\psi \neq 0$, the equations for the internal flow are solved simultaneously for the two velocity components v and w, when u has been eliminated from the equations by using equation (10). The equations are translated from their vector form to scalar notation by utilizing cylindrical coordinates. Then a further transformation is employed with characteristic quantities as the independent variables.

The continuity equation (1) is first written in vector form (the condition of axial symmetry being used) and multiplied by $r/\rho A$:

$$\frac{r}{\rho A}\nabla\cdot\left(\rho\frac{A}{r}W\right) = \nabla\cdot W + W\cdot\frac{\nabla\rho}{\rho} + \frac{r}{A}W\cdot\nabla(A/r) = 0$$

For isentropic flow

$$\frac{\nabla\rho}{\rho} = \frac{\nabla h}{a^2}$$

Introduction of E by equation (4) and use of $W \cdot \nabla E = 0$ produces

$$\nabla \cdot W - \frac{W \cdot \nabla W^2/2}{a^2} + \frac{\omega^2 rv}{a^2} + \frac{r}{A}\left(v \frac{\partial A/r}{\partial r} + w \frac{\partial A/r}{\partial r}\right) = 0$$

This expression finally reduces to

$$\left(1 - \frac{w^2}{a^2}\right) w_z - \frac{wv}{a^2}(v_z + w_r) + \left(1 - \frac{v^2}{a^2}\right) v_r - \frac{v}{a^2}\left(\frac{u^2}{2}\right)_r - \frac{w}{a^2}\left(\frac{u^2}{2}\right)_z +$$

$$\frac{v}{r}\left(1 + \frac{\omega^2 r^2}{a^2}\right) + \frac{r}{A}\left[v \frac{\partial(A/r)}{\partial r} + w \frac{\partial(A/r)}{\partial z}\right] = 0 \qquad (15)$$

In cylindrical coordinates, equation (9) becomes

$$w_r - v_z + f_r \mu_z - f_z \mu_r = \rho A \frac{dE}{d\psi} \qquad (16)$$

If equation (14) is now substituted into equations (15) and (16), there results for continuity

$$\left(1 - \frac{w^2}{a^2} + \frac{ruw f_z}{a^2}\right) w_z + \left(\frac{ruv f_z}{a^2} - \frac{wv}{a^2}\right) w_r + \left(\frac{ruw f_r}{a^2} - \frac{wv}{a^2}\right) v_z +$$

$$\left(1 - \frac{v^2}{a^2} + \frac{ru f_r v}{a^2}\right) v_r + \frac{ru}{a^2}\left(w^2 f_{zz} + 2wv f_{rz} + v^2 f_{rr}\right) +$$

$$\frac{v}{r}\left(1 + \frac{\omega^2 r^2}{a^2} - \frac{u^2}{a^2}\right) + \frac{r}{A}\left[v \frac{\partial}{\partial r}(A/r) + w \frac{\partial}{\partial z}(A/r)\right] = 0 \qquad (17)$$

and for the equation of motion

$$\left(1 + r^2 f_z{}^2\right) w_r + r^2 f_z f_r (v_r - w_z) - (1 + r^2 f_r{}^2) v_z +$$

$$r^2 f_z{}^2 \left[v \frac{\partial}{\partial r}\left(\frac{f_r}{f_z}\right) + w \frac{\partial}{\partial z}\left(\frac{f_r}{f_z}\right)\right] - 2\mu \frac{f_z}{r} - \rho A \frac{dE}{d\psi} = 0 \qquad (18)$$

Use of Characteristic Variables

Statement of basic equations. - The method of reference 3 is applied to equations (17) and (18). The object is to find two alternative equations with new variables ξ and η, instead of z and r, such that each equation (corresponding to equations (17) and (18)) contains derivatives with respect to only one of the independent variables. Two additional equations are required to find the position coordinates z and r in terms of the characteristic coordinates ξ and η. There are two characteristic slopes dr/dz, ζ_+ and ζ_-, the first corresponding to ξ varying and η constant, the second to ξ constant and η varying. If ζ represents either of these slopes and σ represents either of the coordinates corresponding to the appropriate ζ, the results are

$$r_\sigma = \zeta\, z_\sigma \tag{19}$$

$$\zeta = \frac{1}{B}\left[-r^2 f_r f_z - \frac{wv}{a^2} r^2 (\nabla\alpha)^2 \pm \sqrt{r^2 (\nabla\alpha)^2 (M^2 - 1)}\right] \tag{20}$$

(the upper sign of $\pm$ refers to ζ_+, the lower to ζ_-) and

$$Jw_\sigma + Gv_\sigma + Lz_\sigma = 0 \tag{21}$$

where

$$\left.\begin{aligned}
B &= 1 + r^2 f_r{}^2 - \frac{w^2}{a^2} r^2 (\nabla\alpha)^2 \\
M^2 &= \frac{(u^2 + v^2 + w^2)}{a^2} \\
J &\equiv \frac{(w - ruf_z)^2}{a^2} - (1 + r^2 f_z{}^2) \\
G &\equiv (M^2 - 1)\, r^2 f_r f_z + \frac{wv}{a^2} r^2 (\nabla\alpha)^2 \pm \sqrt{r^2 (\nabla\alpha)^2 (M^2 - 1)} \\
L &\equiv -\left(r^2 f_r f_z \zeta + 1 + r^2 f_z{}^2\right) D_1 + \left[\frac{v}{a^2}(ruf_z - w) - \left(1 - \frac{w^2}{a^2} + \frac{ruw}{a^2} f_z\right)\zeta\right] D_2 \\
D_1 &\equiv \frac{ru}{a^2}\left(w^2 f_{zz} + 2wvf_{rz} + v^2 f_{rr}\right) + \frac{v}{r}\left(1 + \frac{\omega^2 r^2}{a^2} - \frac{u^2}{a^2}\right) + \frac{vr}{A}\frac{\partial(A/r)}{\partial r} + \frac{wr}{A}\frac{\partial(A/r)}{\partial z} \\
D_2 &\equiv r^2 f_z{}^2 \left[v \frac{\partial}{\partial r}\left(\frac{f_r}{f_z}\right) + w \frac{\partial}{\partial z}\left(\frac{f_r}{f_z}\right)\right] - 2(u + \omega r) f_z - \rho A \frac{dE}{d\psi}
\end{aligned}\right\} \tag{21a}$$

Equation (20) for ζ shows that the system is hyperbolic if $M^2 > 1$.

In the homogeneous equations ($D_1 = D_2 = 0$), the coefficients L_+ and L_- (corresponding to ζ_+ and ζ_-) are zero; consequently, in the hodograph plane the slope of the characteristics would be given by $\frac{dv}{dw} = -\frac{J}{G}$. In plane flow, J/G is a function of v and w only, and this equation may be integrated and the hodograph solutions tabulated in advance of application to any particular problem that may arise. In the present circumstances, however, J/G also involves the position coordinates, and $D_1 \neq 0$, $D_2 \neq 0$. A correspondingly easy method of solution by simple waves is therefore unavailable. Instead, the four ($\sigma = \xi$ or η) equations (19) and (21) are integrated simultaneously in a step-by-step procedure.

Method of computation. - In figure 1, conditions are supposedly known at P_1 and P_2, and conditions are to be computed at P_3. Then equation (19) in difference form is

$$r_3 - r_1 = (z_3 - z_1)\zeta_+ \tag{22}$$

$$r_3 - r_2 = (z_3 - z_2)\zeta_- \tag{22a}$$

This system may be solved for r_3 and z_3. Then similarly for equation (21), the difference form is

$$J(w_3 - w_1) + G_+ (v_3 - v_1) + L_+ (z_3 - z_1) = 0 \tag{23}$$

$$J(w_3 - w_2) + G_- (v_3 - v_2) + L_- (z_3 - z_2) = 0 \tag{23a}$$

The subscript + indicates that η is constant and the subscript - indicates that ξ is constant. In equation (22) and (23a) the coefficients ζ, J, G, L are averages between values for the points P_1 and P_3. For the first approximation, only the values at P_1 are known and these values are used.

When approximate velocity components and position coordinates are thus determined for P_3, the coefficients ζ, J, G, L may be computed there and averaged for a better approximation of the position coordinates and the velocity components at P_3. This process is repeated as

often as necessary to arrive at an answer of satisfactory accuracy. The smaller the interval, the quicker the convergence to the solution. In each stage of the process, if $dE/d\psi \neq 0$, then ψ_3 must be computed from

$$\psi_3 - \psi = \int_z^{z_3} (\psi_r \zeta + \psi_z) dz = \int_r^{r_3} (\psi_r + \psi_z/\zeta) dr$$

From the value of ψ_3, $dE/d\psi$ at P_3 may be found.

BOUNDARY CONDITIONS

General

The discussion in the previous section implies that boundary conditions are known on a curve C containing points such as P_1 and P_2, and that the solution is then extended into a region containing points such as P_3. The shape of the blades and $E(\psi)$ are assumed known in that region. On the curve C, there are known in addition the values for w and v, from which all other variables (such as $dE/d\psi$, ψ, u, ρ, a^2, and so forth) may be computed. Suppose the initial curve is such that the characteristic curves intersect it at two points such as A and D or A and E in figure 2. Then by equation (21), there is a relation between the variables at A and D that does not permit the independent specification of the variables v and w at A and D. Similarly if two characteristics passing through two boundary points reach a third boundary point, then another degree of freedom is lost. In figure 2, if two variables are prescribed in AB and EF, then one variable may be prescribed on BC and DE, and none on CD.

Tip Conditions

The supersonic impeller has a high pressure ratio per stage and a large air-handling capacity per unit of frontal area. In order to maintain the large capacity, the tip radius at the entrance should be at least as large as the exit. In order to provide a maximum work output with a minimum turning, the exit tip radius should be at least as large as the entrance tip radius. A reasonable shape for the tip streamline is therefore a surface of constant radius, although smaller radii between the entrance and the exit might be useful in order to affect the internal flow. If the casing shape is selected, then, as it is also a streamline,

the ratio v/w is specified. Selection of the velocity or a velocity component remains. This selection may be made by consideration of the blade-to-blade velocity variations and by using some approximate method such as that outlined in the following paragraphs.

In three-dimensional motion (finite number of blades), Kelvin's theorem states that if the absolute velocity is irrotational upstream of the impeller, it will remain so inside the impeller; that is,

$$\nabla \times V' = \nabla \times W' + 2\omega k = 0$$

where the prime indicates velocities of the nonsymmetric flow. Then

$$\nabla \psi \cdot \nabla \times V' = 0$$

may be reduced to

$$\frac{\partial}{\partial \theta} (W' \cdot \bar{q}) = r \frac{\partial u'}{\partial s} + (u' + 2\omega r)\, \bar{q} \cdot i \tag{24}$$

where $\partial u'/\partial s$ is the arc-length partial derivative of u' along the direction of $\bar{q}$. This equation is now integrated from the pressure surface of one blade to the suction surface of the next in the direction r = constant, z = constant. The variable θ increases by the amount $2\pi A/Nr$, so that

$$(W' \cdot \bar{q})_s - (W' \cdot \bar{q})_p = r \int_{\theta_p}^{\theta_s} \frac{\partial u'}{\partial s}\, d\theta + \bar{q} \cdot i \int_{\theta_p}^{\theta_s} u'\, d\theta + \frac{2\pi A}{Nr}\, 2\omega r \bar{q} \cdot i$$

If it is now assumed that the values of $\partial u'/\partial s$ and of u' averaged across the channel are equal to the values obtained from the axisymmetric solution, and further that $(W' \cdot \bar{q})_s = |W'_s|$, then

$$|W'_s| - |W'_p| = \left[\frac{\partial u}{\partial s} + \left(\frac{u}{r} + 2\omega\right) \frac{v}{|\bar{W}|}\right] \frac{2\pi A}{N} \tag{24a}$$

if the relation

$$v/|W| = i \cdot \bar{q}$$

is utilized. In this equation all the velocity components without subscripts are obtained from the axisymmetric solution. If

$$|W'_s| + |W'_p| = 2|W|$$

is assumed or some other connection between $|W'_s|$, $|W'_p|$, $|W|$, and the impeller geometry, then the blade surface velocities at the casing may be obtained with that relation and equation (24a). The distribution of $|W|$ at the casing may therefore be selected on the basis of obtaining a desired blade-surface velocity distribution or distribution of u.

Suppose that, in some manner, all the variables have been selected at the case (curve BC in fig. 3(a)). The flow is then uniquely determined in the region BP_1C enclosed by the casing and two characteristic lines. If the flow is also prescribed at the leading-edge surface BB', then the flow is determined in the extended region $B'BCP_1P_2$. When the characteristic line BP_3 falls inside this region (fig. 3(a)), no difficulty results. If, however, the characteristic $B'P_4$ intersects the casing inside the blade region (fig. 3(b)), then the velocity may not be prescribed on the curve BP_4 (refer to discussion of fig. 2), or alternatively, only one of the velocity components may be prescribed on BB'. (BB' is not a streamline.) Similar considerations are valid on the curve CC' at the exit.

The selection of values for the variables v and w on the entrance edge BB' must be made by joining the solution for the flow in the region ABB'A' with that for the flow in the blade region BCC'B'. Because the blades may deflect the air at BB' discontinuously and because the effect of thickness may be felt by the air in a discontinuous manner, the discontinuities in the flow should be evaluated. A method for making this estimate follows:

The angle β is defined as the angle between the meridional projection of the blade leading edge and the z-axis (fig. 3(a)). The conditions outside the blade region are designated by subscript zero, inside the blade region by no subscript. Then across the surface BB' the equation of continuity yields

$$\rho_0 (w_0 \sin \beta - v_0 \cos \beta) = \left(1 - \frac{Nt}{2\pi r}\right) \rho (w \sin \beta - v \cos \beta) \qquad (25)$$

The discontinuity in blade thickness can cause no force in the entrance surface BB', and the blades can exert no force in the blade surface. Therefore, no force and no discontinuity in momentum exist in the direction of the curves representing the intersection of these two surfaces; that is

$$(W - W_0) \cdot (i \cos \beta - k \sin \beta) \times \nabla \alpha = 0$$

or

$$r(u - u_0)(f_r \sin \beta + f_z \cos \beta) = (v - v_0) \sin \beta + (w - w_0) \cos \beta \tag{26}$$

There is also available

$$u = - r \left(w f_z + v f_r \right) \tag{27}$$

If the process is assumed isentropic, then

$$\frac{\rho}{\rho_0} = \left(\frac{h}{h_0} \right)^{\frac{1}{\gamma - 1}} = \left(1 + \frac{V_0^2 - V^2}{2h_0} \right)^{\frac{1}{\gamma - 1}} \tag{28}$$

is obtained by utilizing the fact that

$$E = h_0 + \frac{W_0^2}{2} - \frac{\omega^2 r_0^2}{2} = h + \frac{W^2}{2} - \frac{\omega^2 r^2}{2}$$

and that

$$r_0 = r$$

There are then available equations (25), (26), (27), and (28) for finding ρ, u, v, and w. The initial values of f_r and f_z may be chosen from these equations to obtain desired relations between the velocity components outside and inside the blade regions.

Applications of Method of Characteristics

In the examples computed in this section, the conditions for which solutions are obtained vary. The purpose of these solutions is to find the effect of some variations of prescribed conditions on the resultant

flow. For all the examples, $dE/d\psi = 0$; the flow is vortex-free upstream of the impeller; at the leading and trailing edges the radial component v of the velocity is zero; and the blades contain radial elements ($f_r = 0$). Relative Mach number at the conjunction of the leading edge of the blade and the impeller casing is 1.94. Except in example VI, the value of the blade angle with respect to the axial direction is zero at the exit ($f_z = 0$). The other conditions are summarized in the following table:

Example	Entrance				Case velocity	Turning rate	Sweep-back (deg)	Blade thickness
	Pre-rotation, $(u+\omega r)r$	Axial inlet velocity	Tip speed	Blade angle at tip (deg)				
I	0	$0.85a_1$	$1.68a_1$	-61.8	(a)	0 to maximum to 0	0	0
II	$-0.3a_1r_t$	$0.835a_1$	$1.44a_1$	-64.4	$1.94a_1$	0 to maximum to 0	45	0
III	$-0.3a_1r_t$	$0.835a_1$	$1.44a_1$	-64.4	$1.94a_1$	Twice example II	45	0
IV	$-0.3a_1r_t$	$0.835a_1$	$1.44a_1$	-64.4	(b)	Twice example II	45	0
V	$-0.3a_1r_t$	$0.835a_1$	$1.44a_1$	-64.4	(b)	Twice example II	45	(c)
VI	$-0.3a_1r_t$	$0.835a_1$	$1.44a_1$	-64.4	(d)	0 to maximum	10	0

[a]Determined by conditions at leading edge to $z/r_t = 0.356$; held constant at 2.1a from $z/r_t = 0.356$ to 1.0.

[b]Constant at 1.94a to $z/r_t = 0.25$; decreased to 1.4a ($= 1.6a_1$) at exit.

[c]Zero from $z = 0$ to $z/r_t = 0.25$; from $z/r_t = 0.25$ to $z/r_t = 0.5$ the correction for blade thickness is

$$A = r \exp\left\{-\frac{0.1}{r}\left[1 - \cos 8\pi\left(\frac{z}{r_t} - 0.25\right)\right]\right\}$$

[d]Determined by leading edge; initial value, 1.94a.

Example I. - The results of the computation for the first example are summarized in figure 4, which shows streamlines, contours of constant Mach number and constant energy level, and some of the characteristics of the ξ-family, which intersect the leading edge. Because of the intersection of the characteristics from the leading edge with the tip of the blades, there is no control over the Mach number, as the blade shape was prescribed by

$$r \frac{d\theta}{dz} = - r \frac{df}{dz} = - 1.04 \frac{r}{r_t} \left(1 + \cos \pi \frac{z}{r_t}\right)$$

The Mach number at the case rises to a maximum of 2.1 at $z/r_t = 0.356$, and is then assigned a constant value. By equation (4), the stagnation enthalpy H ($\equiv h + V^2/2$), which measures the energy of the gas, increases with z at the rate

$$\frac{\partial H}{\partial z} = \omega r \frac{\partial u}{\partial z}$$

At the case $v = 0$, and therefore, from equation (14) and $W^2 = u^2 + w^2$,

$$\frac{\partial H}{\partial z} = \frac{\omega r}{|W|} \left(u|W|_z - \frac{r w^3}{|W|} \frac{d^2 f}{dz^2}\right)$$

This expression shows that the rate of work input is increased by increasing the rate of blade turning and decreased by increase in W. Figure 4 indicates that the rate of turning of the blade is too small in the beginning of the impeller and that as a consequence nearly all the work input is concentrated in the back end of the impeller. This condition is aggravated by the acceleration of the gas in the initial portion ($u|W|_z < 0$ because $u < 0$). Increasing the turning rate, however, will open the flow area and cause $|W|$ to increase unless the area is controlled by blade thickness.

A great disparity of work exists between the root and the tip; the values for $\Delta H/a_1^2$ are 0.65 and 2.5 at the exit. For isentropic compression, the corresponding ratios of outlet to inlet stagnation pressures are 2.48 and 9.0 for the root and the tip, respectively. The Mach number at the root at the exit ($z = r_t$, $r = 0.507\ r_t$) is in the neighborhood of 2.25, and a maximum value of about 2.5 is reached at $z = r_t$, $r = 0.70\ r_t$. Subsonic Mach numbers are reached in the region $0 < z/r_t < 0.3$. The solution could not be extended into this region.

If the velocity were caused to decrease at the exit ($z = r_t$) by decreasing the velocity at the case ($r = r_t$) in the rear part of the impeller ($0.356 < z/r_t < 1.0$), then the mass-flow density at the exit would increase with the decrease in velocity and the required flow area would decrease. Termination of the hub would be expected, not at $r = 0.507\ r_t$, but at some larger value where the work output would be higher. Another method of reducing the blade height at the exit and thereby reducing the work variation there would consist in relaxing the condition of $v = 0$ and utilizing some other relations that would correspond to lower Mach numbers. Two variables or relations could also be prescribed at the exit, but conditions on the blade tip ($r = r_t$) could not be specified for some region near the back of the impeller. In this respect the entrance and exit conditions would be similar.

Example II: Prerotation of gas. - In order to maintain supersonic flows throughout the impellers so that the flow could be computed, the relative entrance Mach number at the blade root for example II was increased by assuming an initial counterrotation. The rotative speed had to be reduced from $1.68a_1$ to $1.44a_1$ to maintain the work output, the relative Mach number at the leading-edge tip, approximately the same blade angle there, and the same axial velocity component at the inlet. This reduction had a further beneficial result of reducing the absolute Mach number at the exit for a given relative velocity axially directed. The condition of $z = \text{constant}$ for the leading edge cannot be maintained for shockless entry with radial blade elements and a counterrotating free vortex entering the blade system. The sweep angle β chosen for this example was 45°, enough to permit free selection of $W = 1.94a$ over the entire blade tip, because the characteristic curves from the leading edge do not interfere with boundary conditions on the casing. The reduction in velocity at the casing reduces the blade height at the exit and the work-output variation there.

In order to examine deviations from an example more nearly representative of a good design, the velocity at the blade tip for example II was not maintained the same as in example I, and consequently the differences between examples I and II are not ascribable solely to inlet prerotation. Comparison of the effect on rotative speed (for the same turning at the tip and the same work output) and on diffusion at the blade roots is, however, valid.

The results of the computations are shown in figure 5. In this example, the turning rate is predetermined in the region $-0.5 < z/r_t < 0$ by the velocity distribution upstream of the leading edge, the condition of radial blade elements, and the slope of the leading edge. The

turning rate is continuous at $z = 0$, and satisfies the equation

$$\frac{d}{dz}\left(\frac{rd\theta}{dz}\right) = 3.008 - 2.298\,(3z - 1)^2 \qquad (0 < z/r_t < 1/3)$$

$$= 3.008\left[1 - 1/4\,(3z - 1)^2\right] \qquad (1/3 < z/r_t < 1)$$

Compared with the first example, the work-input rate at the blade tip is greater in the initial section; however, the work distribution is still unsatisfactory. The exit blade height is also much less, with the result that the work input is much more nearly equalized; at the root, the value of $\Delta H/a^2$ is 1.8, whereas, at the tip, the value is 2.5. These values correspond to stagnation pressure ratios of 5.2 at the root and 8.35 at the tip. This variation could be reduced by sweeping back the trailing edge to provide space for additional work input at the hub streamline. This sweepback is more feasible with the smaller blade height and work variation of the second example than for the first example.

Example III: Effect of turning rate. - In order to reduce the size of the impeller by increasing the turning rate, example III was computed with twice the blade turning rate of example II for $z > 0$ and with the same over-all work output. One result is the greater diffusion on the hub, where a minimum Mach number of 1.2 is reached instead of 1.4 as in the previous example (See fig. 6). The increased diffusion probably results from the increase in hub curvature, which in turn is caused by the shorter axial distances required for the changes. Another result is the increased height of the blade at the exit, and an increase in the exit Mach number from 2.3 to 2.7. The increased streamline curvature also accounts for the higher exit velocity and this higher velocity in turn explains the larger blade height. The characteristic line through the casing at the exit ($r = r_t$, $z = 0.5\ r_t$) intersects the hub at $z = 0.155\ r_t$. The characteristics through the remaining portion of the hub ($z > 0.155\ r_t$) are affected by conditions at the exit ($z = 0.5\ r_t$) where the velocities increase with decreasing radius. The result is a large increase in velocity at the blade hub in the region $z > 0.155\ r_t$.

Example IV: Effect of diffusion at casing. - In the next example, all conditions remained the same as in the third example except that the prescribed velocity at the case was varied smoothly from the value of 1.94a at $z = 0.25\ r_t$ to 1.40a at $z = 0.5\ r_t$. The desired reduction has been obtained in blade height and work-output variation, but the discharge velocity has a large value of 2.6a (fig. 7). It may

therefore be concluded that the alternative of directly prescribing a condition with low relative velocities at the exit would have been more effective than prescribing conditions at the blade tip for reducing the blade height at the exit.

A new phenomenon has also arisen in that the characteristics passing through $z = 0.5\ r_t$, $r = 0.92\ r_t$; and $z = 0.5\ r_t$, $r = 0.893\ r_t$ intersect at $z = 0.397\ r_t$, $r = 0.832\ r_t$. At this point, the Mach number changes discontinuously from 2.13 to 2.43 and the streamline inclination to the axis changes from 14.9° to 7.4°. This single point does not represent the full extent of this difficulty. Actually, there is a region bounded by a curve in which two solutions are obtained; each solution is determined by a different region of the boundary. Consequently, the boundary conditions are incompatable with obtaining a single-valued continuous solution. This situation is analogous to the Prandtl-Meyer flow, where the characteristics intersect at the corner. If a computation were started for a simple two-dimensional supersonic flow from a streamline shape and from the velocity distributed thereon, which were exactly the same as on one of the streamlines of a Prandtl-Meyer flow around a corner, then, when the solution was extended toward the corner, the characteristics would intersect at the corner in the manner of figure 7. The intersection on figure 7 can be taken to represent a physical boundary to the fluid in that the streamline passing through that point would be taken for the hub shape. Only 90 percent of the flow ($\psi = 0.9$) could be accommodated in the impeller of example IV if continuous flow with the imposed boundary conditions were required. An obvious method of increasing the flow is to increase the slope of the characteristic lines at the exit for $r < 0.9\ r_t$. This increase could be accomplished by decreasing the relative velocities there and discarding the condition $v = 0$ to obtain a shorter blade height.

Example V: Increasing blade thickness. - In none of the examples computed so far was blade thickness considered. An obvious effect of increasing blade thickness is to decrease the velocity in a region where there is no independent control of the velocity (such as the region $z < 0.35\ r_t$ in example I, fig. 4). This phenomenon provides the degree of freedom required in such regions to control the relative velocity $|W|$ as well as the surface velocities $|W_s|$ and $|W_p|$. In regions where the velocity $|W|$ at the blade tips is under control (the entire tip sections for examples II, III, IV), altogether different effects may be expected. The effect of thickness under these circumstances was investigated by computing another example with a cosine-like bump in the blade thickness starting at $z = 0.25\ r_t$.

(See the previously presented table of boundary conditions.) The maximum thickness was reached at $z = 0.375\ r_t$. At $r = r_t$ the thickness is 20 percent of the blade spacing, and at the hub the value is 25 percent. The results of the computation are shown in figure 8. The effect of the bump is not felt upstream of the characteristic with positive slope passing through $z = 0.25\ r_t$, $r = r_t$. The most obvious effect is a decrease of flow Mach number in the region of increasing thickness (and inward from the casing, where the velocity is not preassigned), as might be expected from one-dimensional theory. At $z = 0.25\ r_t$ and $z = 0.375\ r_t$, the change in blade height is about 10 percent as compared with example IV. Another effect of thickness is to be seen in the waviness of the hub streamline in the region $0.15 < z/r_t < 0.25$ where the thickness has not yet started to increase. This bump may be traced in other streamlines along the characteristic running through the point of maximum thickness at the case $(r = r_t,\ z = 0.375\ r_t)$. The effect of the bump on the hub is therefore to increase the local velocity by curvature in order to hold the required velocity at the casing; this action from hub to casing takes place along the characteristic line as simple waves in two dimensions, and the velocity is seen to have increased all along this characteristic line. The intersection of the characteristics and the double-valued solution occur near the exit over a considerably larger portion of the flow than in the previous example. In this example also, if a lower velocity were prescribed at the exit, a unique solution would be obtained. It would also be feasible to carry out this idea and at the same time to prescribe another condition (such as $v = 0$) provided that one were willing to lose control of the condition at the back end of the casing $(r = r_t)$ in a manner analogous to that used at the front end of example I.

Example VI: Effect of leading-edge sweep. - It is of more technical interest, however, to carry out this scheme at the entrance, for then the leading-edge sweep may be reduced from 50 percent of the axial depth of the machine to considerably less. A computation of the inlet flow conditions for such an impeller is shown in figure 9, where the conditions at the leading edge are the same as for example III. The blade shape is different, with the second derivative of angle $\frac{d^2\theta}{dz^2} = -\frac{d^2f(z)}{dz^2}$ constant. Also, the velocity at $r = 1.0$ cannot be prescribed. Only in the region enclosed by the casing and leading-edge characteristics was the computation completed. The result (fig. 9) shows a large increase in Mach number, especially at the blade tip. Because of this increase, the blade turning accomplishes no work in the beginning of

the impeller, but shows a region of energy abstraction from the air; the initial negative rotational component becomes more negative as the air turns axially and the velocity increases as in example I. The situation is quite different at the back end where the blade angles approach zero and the tangential component does likewise; all the work input is concentrated in the back end of this impeller as in the other examples. Postponement of work input to the back end of the impeller is to be expected in any case where the velocity is increasing as the blades turn toward the axial direction, or if the velocity decreases as the blades turn past the axial direction. Internal flow and work distribution could be considerably improved in this example by increasing blade thickness in the region of large velocity increase.

CONCLUSIONS

General equations developed for isentropic, axisymmetric flows in rotating impellers with any given blade shapes showed that the blade-force term can be eliminated and solved for, if desired, after the flow solution is completed. Further, if the flow upstream of the impeller is vortex-free, then a potential function of only radial and axial distances exists, which may be used to find the projection of the absolute velocity on the blade surface.

For supersonic flow, the method of characteristics was used to compute the flow for several examples with radial blade elements and vortex-free inflow. These examples show that

(1) With zero radial inflow, the influence of the leading edge and the blade turning on the casing velocity in regions where this velocity cannot be prescribed in advance causes an increase in velocity and a reduction of blade loading and work input in the initial portion of the compressor. These effects can be compensated for to some extent by increasing blade thickness.

(2) Sufficient leading-edge sweepback adds a degree of freedom to the boundary conditions at the blade tips, and therefore permits a more constant or a decreasing velocity inside the impeller.

(3) Reduction in the exit velocity results in a shorter blade height and a more uniform distribution of work input at the exit.

(4) Increase in the rate of turning causes more rapid hub curvatures and consequently larger internal velocity gradients. Diffusion on the hub is therefore greater in the initial part of the impeller, and a lower velocity minimum is reached there, whereas the gas velocity

at the hub near the exit reaches larger values. This situation requires larger blade heights at the exit with a larger exit velocity at the root and greater variation of work output from root to tip. Diffusion of the gas velocity at the tip will moderate this effect, as will also a relaxation of the condition zero radial velocity at the exit and the substitution of a condition giving lower exit velocities.

(5) Not every set of boundary conditions results in a continuous, single-valued solution in the region of interest. In the examples considered, a relaxation of the condition zero radial velocity at the exit would have permitted another condition giving lower velocities there. This condition would have eliminated the region of the double-valued solution and given a shorter blade and a more nearly equalized work output.

(6) The effect of variations in blade thickness in regions where velocity is also prescribed at the blade tip is to change the velocity as in one-dimensional flow but not by the same amount, for there is some compensation by variations in blade height. The prescribed velocity and thickness require hub curvatures that cause velocity changes to be projected like simple waves on characteristic curves. It is therefore possible to find regions of increased velocity when the blade thickness is increased.

Lewis Flight Propulsion Laboratory,
National Advisory Committee for Aeronautics,
Cleveland, Ohio, January 24, 1951.

APPENDIX - SYMBOLS

The following symbols are used in this report:

A	$r - Nt/2\pi$
a	sonic velocity of gas
a_1	sonic velocity of gas at conjunction of leading edge and impeller case
a^*	critical speed of gas upstream of impeller
B	an abbreviation (see equations (21a))
D_1, D_2	abbreviations (see equations (21a))
E	sum of stagnation enthalpy and potential energy of gas (specific) in moving coordinates $\left(\equiv h + \frac{W^2}{2} - \frac{\omega^2 r^2}{2}\right)$
F	distributed blade force per unit mass of fluid (a vector)
f	part of blade surface function dependent on r and z only ($\alpha = \theta + f(r,z)$)
G	an abbreviation (see equations (21a))
H	absolute stagnation enthalpy ($h + V^2/2$)
ΔH	work input to gas (rise in absolute stagnation enthalpy)
h	static enthalpy of gas (specific)
i	unit vector parallel to curve θ = constant, z = constant ($i = \nabla r$)
J	an abbreviation (see equations (21a))
j	unit vector parallel to curve z = constant, r = constant ($j = r\nabla\theta$)
k	unit vector parallel to curve r = constant, θ = constant ($k = \nabla z$)

L an abbreviation (see equations (21a))

M local relative Mach number $\left(\left|\frac{W}{a}\right|\right)$

N number of blades

p static pressure of gas

$\bar{q}$ unit vector parallel to W

R vector of r

r normal distance from axis of rotation

r_t distance from axis of rotation to blade tip at leading edge

ds arc-length element parallel to W

t blade thickness measured in direction of rotation

u rotational component of relative gas velocity

V absolute gas velocity (a vector) $[iv + j(u+\omega r) + kw]$

v radial component of gas velocity

W relative gas velocity (a vector) $(iv + ju + kw)$

w axial component of gas velocity

z distance measured parallel to axis of rotation

α function for blade surface $(\alpha(r,\theta,z) = \text{constant})$

β angle between meridional projection of leading edge and axis of rotation

γ ratio of specific heats

ζ either ζ_+ or ζ_- in general form of equations

ζ_+ slope of curve for ξ variable, η constant

ζ_- slope of curve for η variable, ξ constant

η one of characteristic coordinates for gas flow in impeller

θ meridional angle (for cylindrical coordinates)

μ absolute moment of momentum $(r(u + \omega r))$

ξ one of characteristic coordinates for gas flow in impeller

ρ gas density

σ either η or ξ in general form of equations

Φ velocity-potential function of r and z only that exists for initially irrotational absolute motion

ψ stream function $(\nabla\psi = \rho A j \times V)$

Ω vector form of ω

ω angular velocity of impeller

Subscripts:

0 upstream of impeller

p pressure surface of blade at tip

s suction surface of blade at tip

Subscripts r, θ, z, σ, ξ, η indicate partial differentiation.

REFERENCES

1. Reissner, Hans: Blade Systems of Circular Arrangement in Steady, Compressible Flow. R. Courant Anniversary Volume, Interscience Pub. Inc., 1948, pp. 307-327.

2. Wu, Chung-Hua: A General Through-Flow Theory of Fluid Flow with Subsonic or Supersonic Velocity in Turbomachines of Arbitrary Hub and Casing Shapes. NACA TN 2302, 1951.

3. Courant R., and Friedrichs, K.O.,: Supersonic Flow and Shock Waves. Interscience Pub., Inc., 1948.

4. Brand, Louis: Vector and Tensor Analysis. John Wiley & Sons, Inc., 1948, pp. 190, 194.

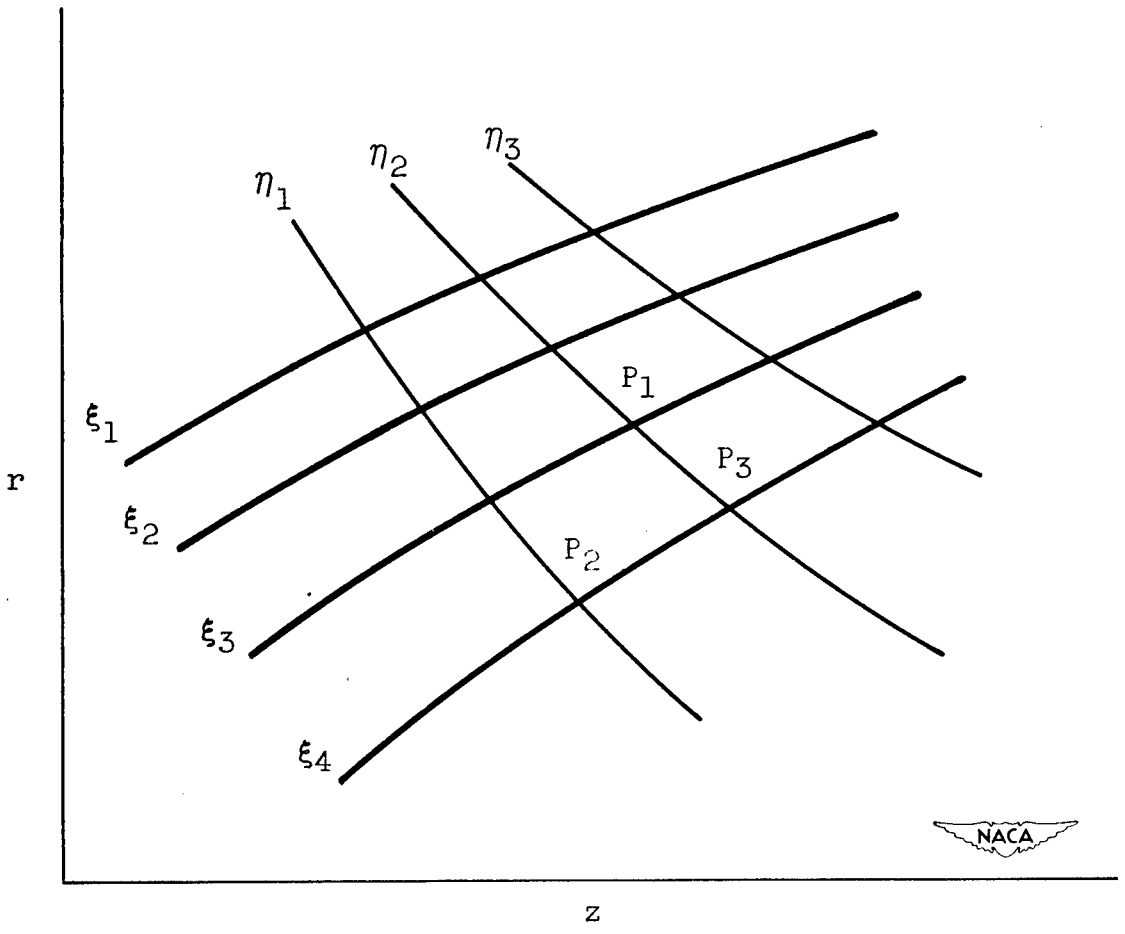

Figure 1. - Characteristic and cylindrical coordinates.

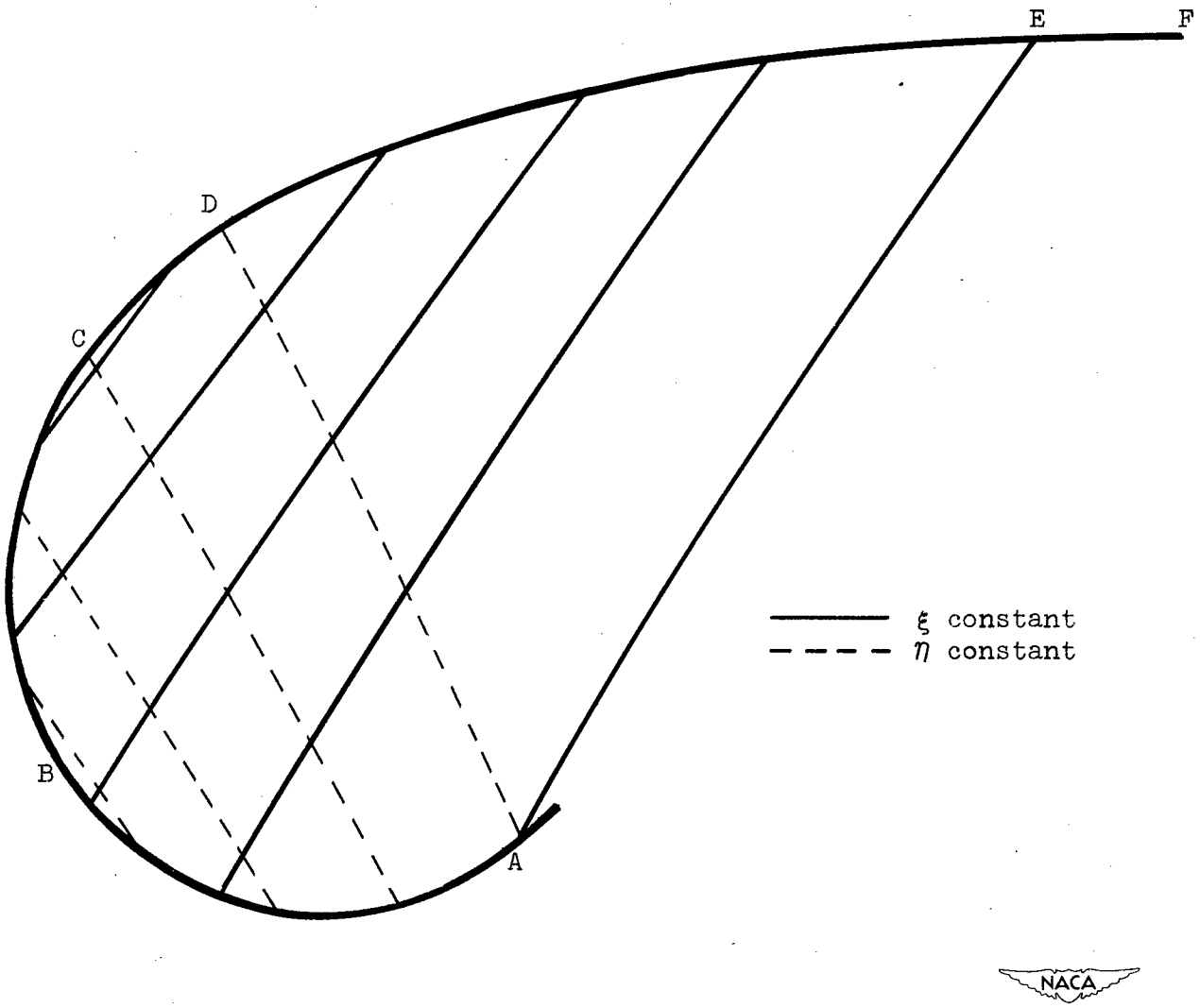

Figure 2. - Relation between shape of boundary and boundary conditions.

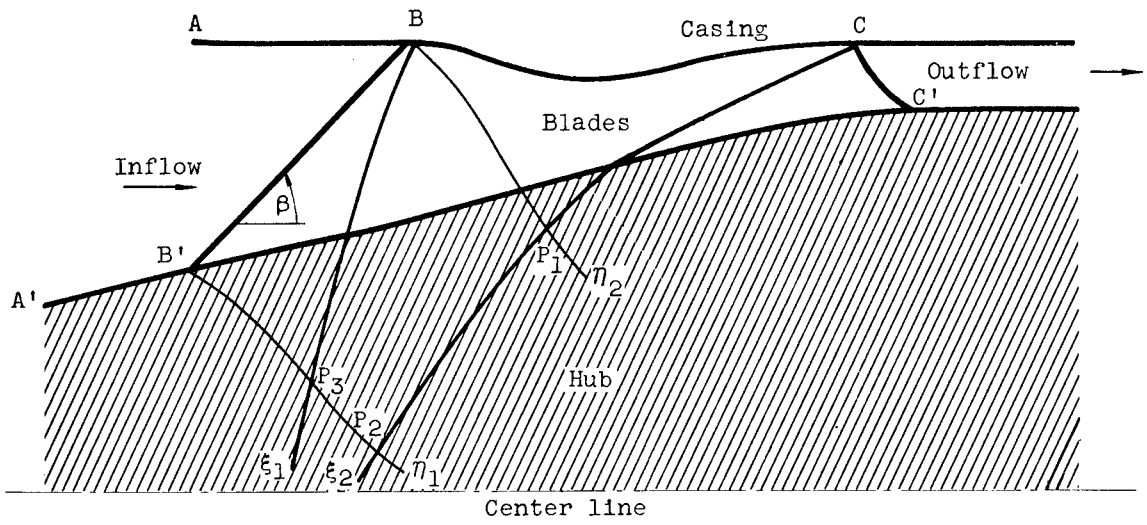

(a) Conditions on B'B and BC unrelated.

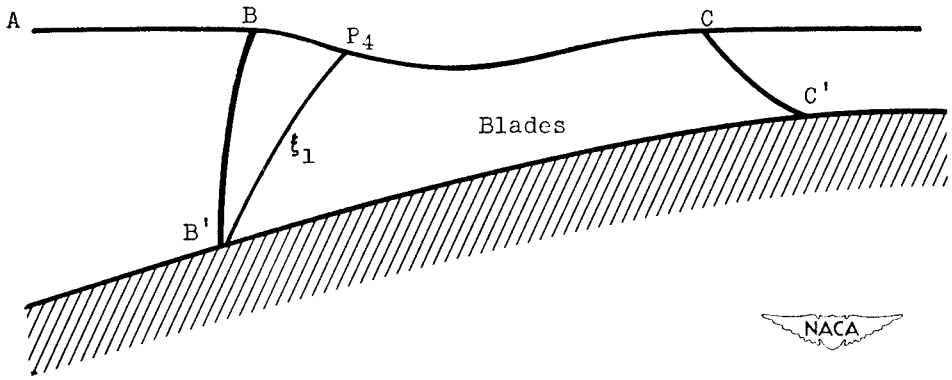

(b) Conditions on B'B related to those on BC.

Figure 3. - Boundary conditions for impeller.

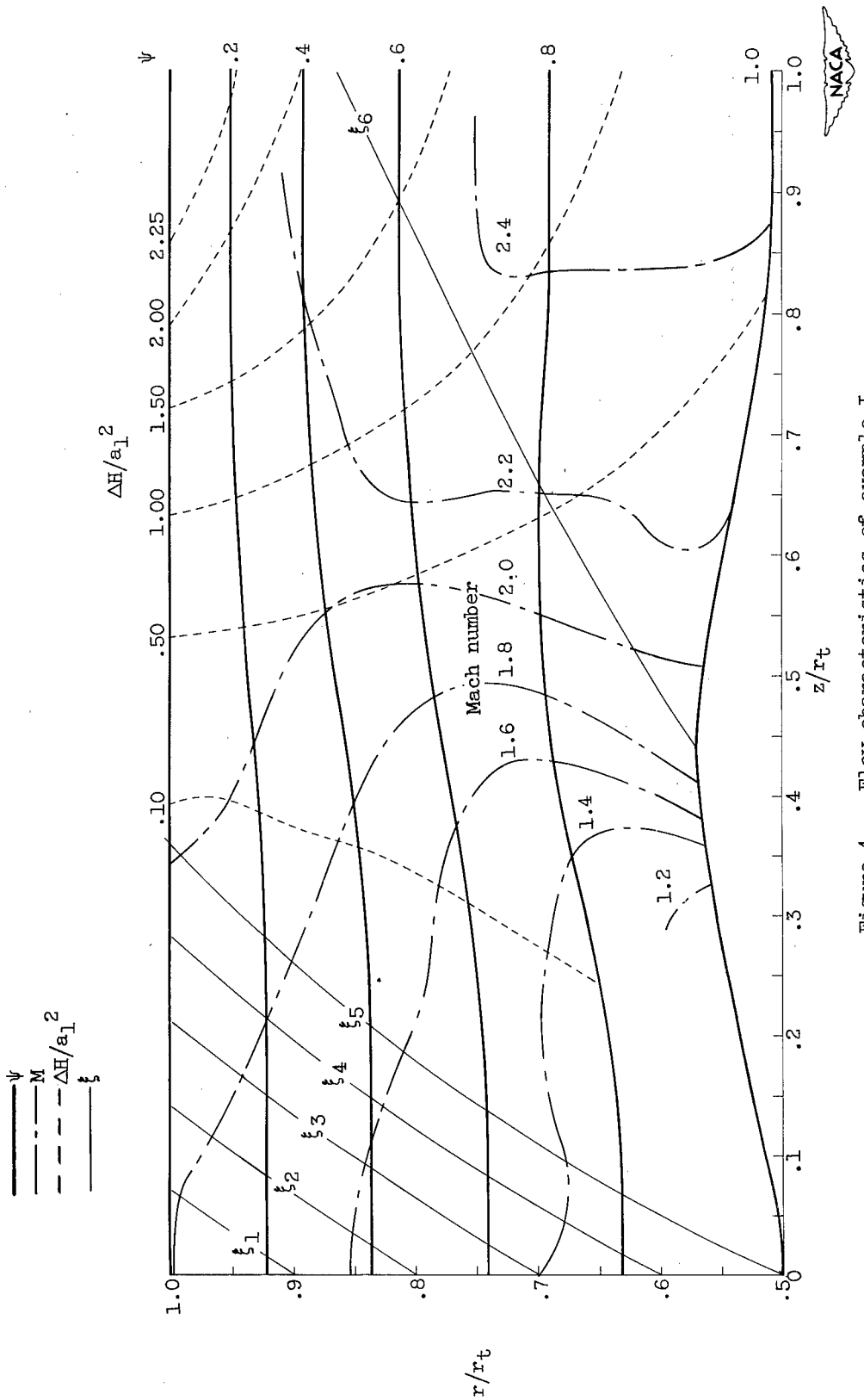

Figure 4. - Flow characteristics of example I.

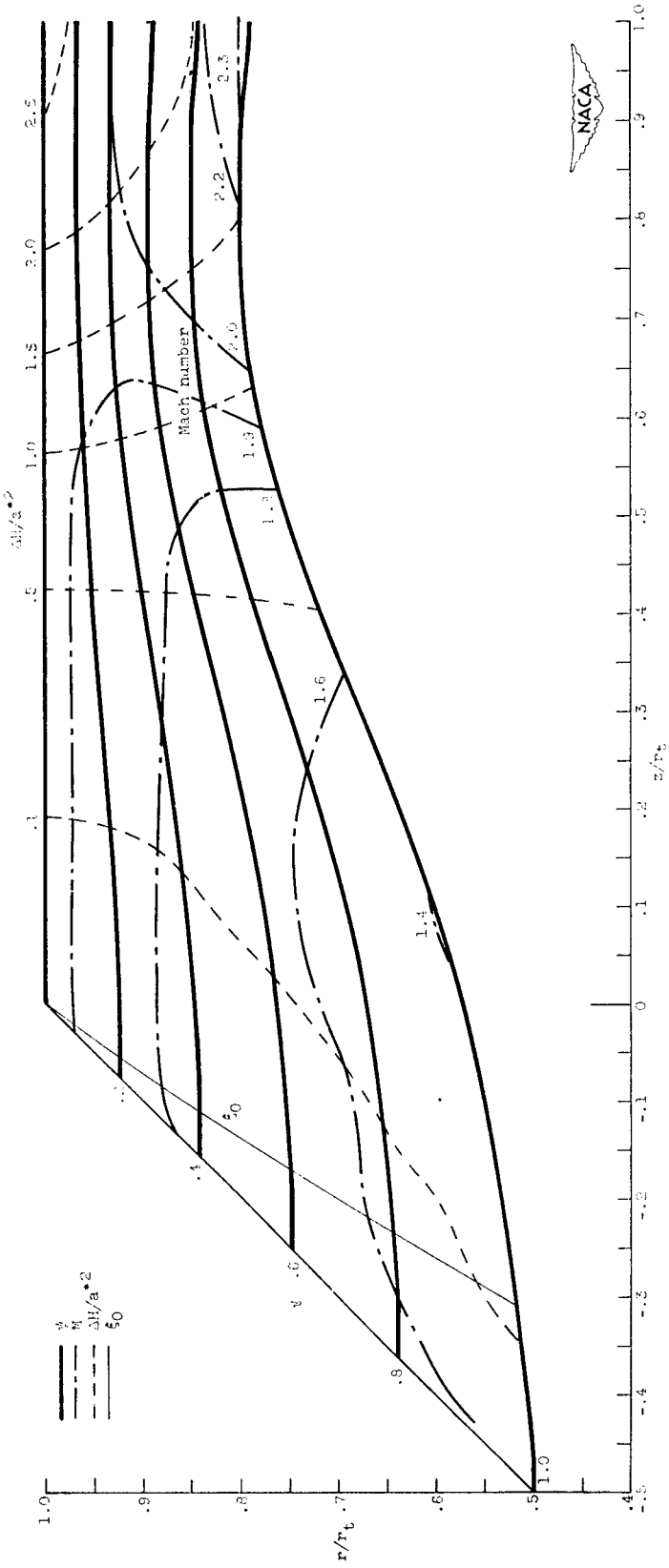

Figure 8. - Flow characteristics of example II.

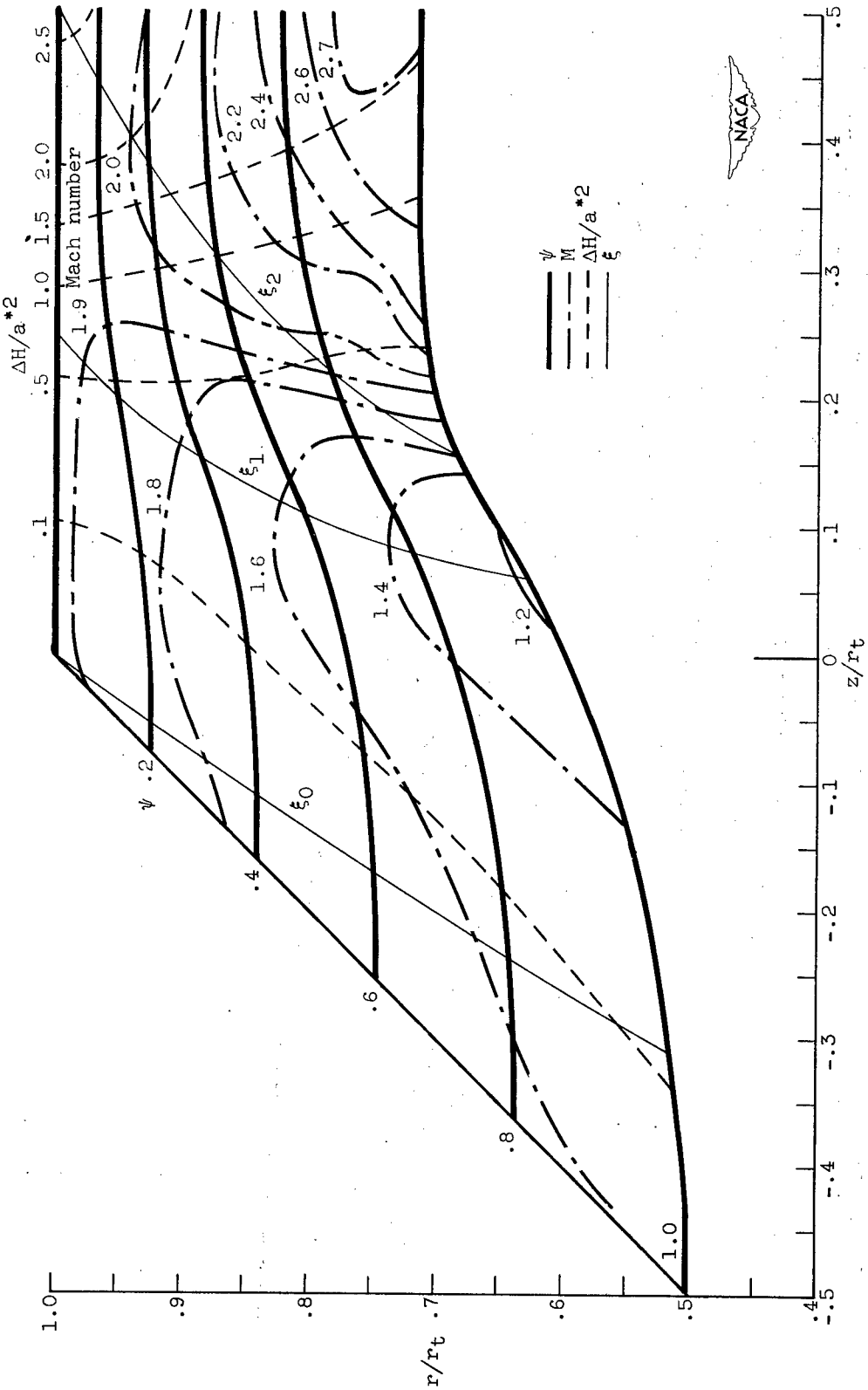

Figure 6. - Flow characteristics of example III.

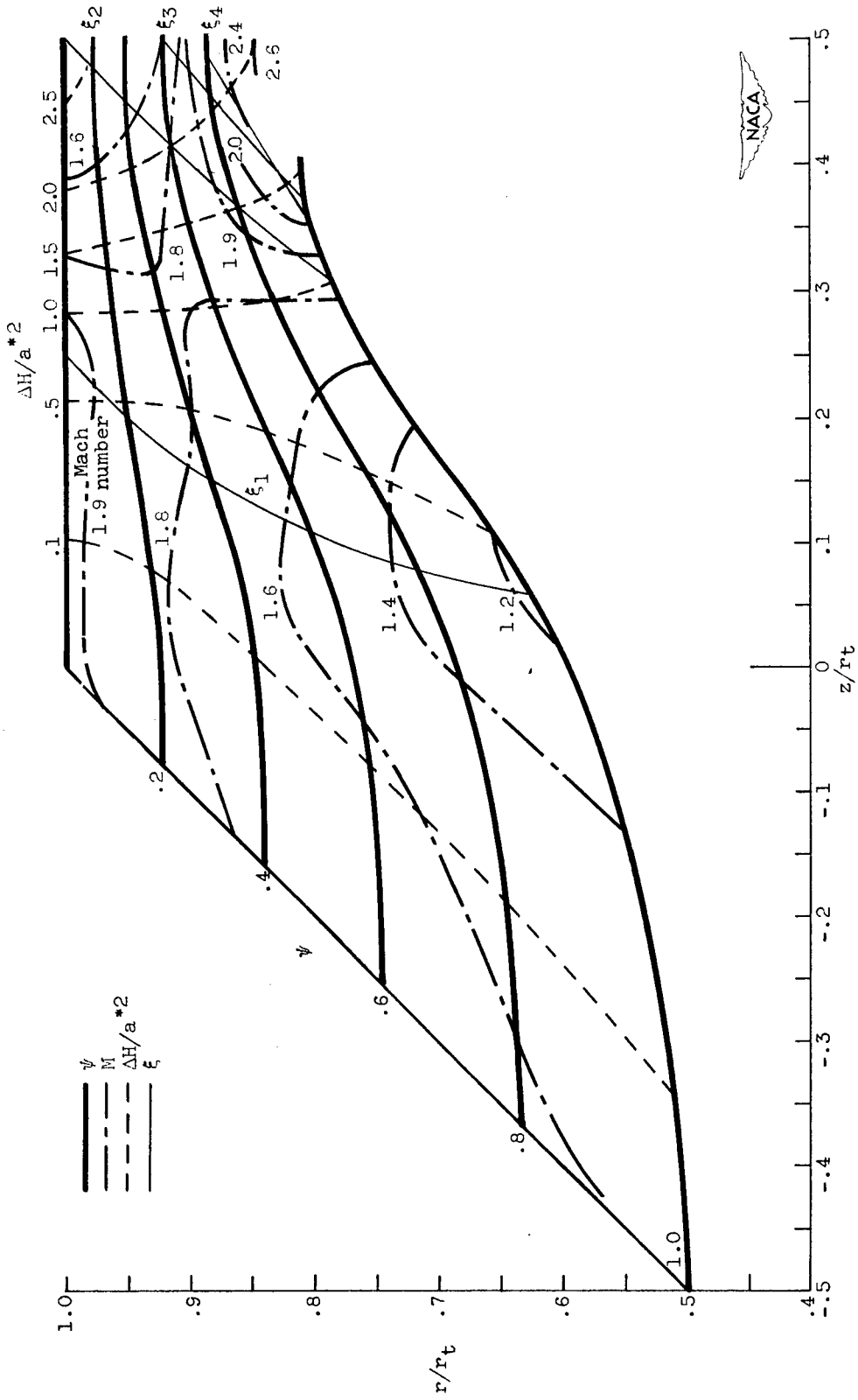

Figure 7. - Flow characteristics of example IV.

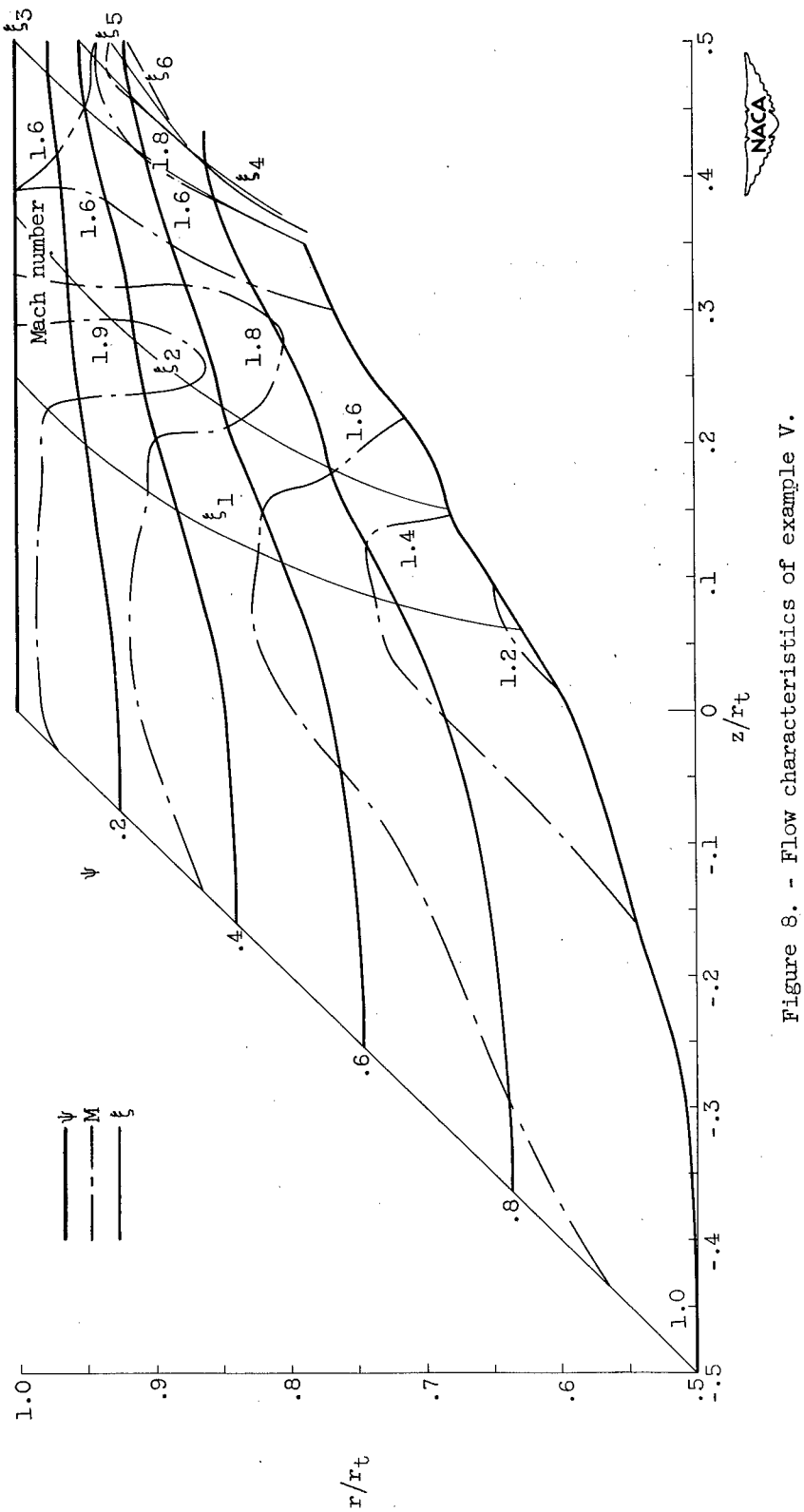

Figure 8. - Flow characteristics of example V.

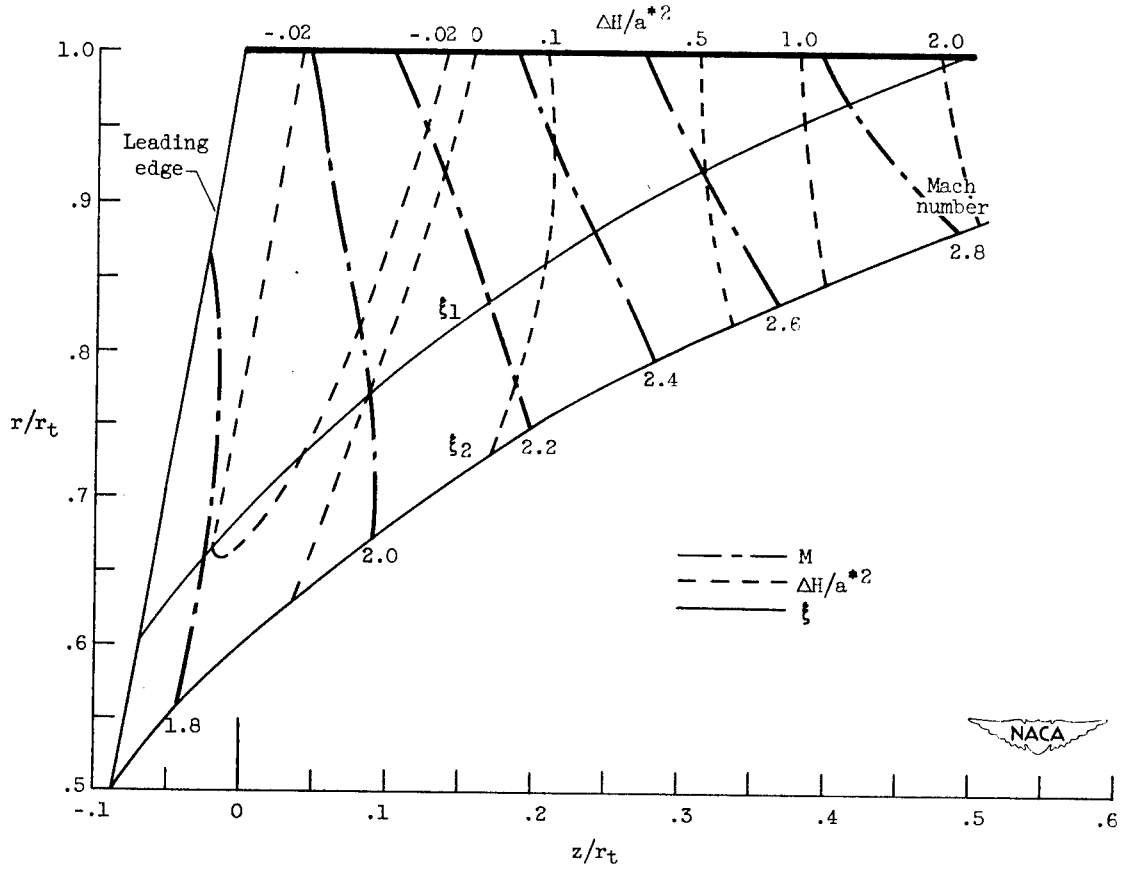

Figure 9. - Flow characteristics of example VI.

NACA TN 2388

National Advisory Committee for Aeronautics. AXISYMMETRIC SUPERSONIC FLOW IN ROTATING IMPELLERS. Arthur W. Goldstein. June 1951. 36p. diagrs. (NACA TN 2388)

General equations are developed for isentropic, frictionless, axisymmetric compressible flow in rotating impellers with blade forces eliminated in favor of the blade-surface function. The characteristic equations for supersonic flow are developed and a computing technique is utilized to find the effect of variations of design parameters on internal flow and work-input distribution.

Copies obtainable from NACA, Washington

1. Flow, Supersonic (1.1.2.3)
2. Compressor Flow Theory and Experiment (3.6.1)
3. Compressors - Mixed Flow (3.6.1.3)

I. Goldstein, Arthur W.
II. NACA TN 2388

NACA TN 2388

National Advisory Committee for Aeronautics. AXISYMMETRIC SUPERSONIC FLOW IN ROTATING IMPELLERS. Arthur W. Goldstein. June 1951. 36p. diagrs. (NACA TN 2388)

General equations are developed for isentropic, frictionless, axisymmetric compressible flow in rotating impellers with blade forces eliminated in favor of the blade-surface function. The characteristic equations for supersonic flow are developed and a computing technique is utilized to find the effect of variations of design parameters on internal flow and work-input distribution.

Copies obtainable from NACA, Washington

1. Flow, Supersonic (1.1.2.3)
2. Compressor Flow Theory and Experiment (3.6.1)
3. Compressors - Mixed Flow (3.6.1.3)

I. Goldstein, Arthur W.
II. NACA TN 2388

NACA TN 2388

National Advisory Committee for Aeronautics. AXISYMMETRIC SUPERSONIC FLOW IN ROTATING IMPELLERS. Arthur W. Goldstein. June 1951. 36p. diagrs. (NACA TN 2388)

General equations are developed for isentropic, frictionless, axisymmetric compressible flow in rotating impellers with blade forces eliminated in favor of the blade-surface function. The characteristic equations for supersonic flow are developed and a computing technique is utilized to find the effect of variations of design parameters on internal flow and work-input distribution.

Copies obtainable from NACA, Washington

1. Flow, Supersonic (1.1.2.3)
2. Compressor Flow Theory and Experiment (3.6.1)
3. Compressors - Mixed Flow (3.6.1.3)

I. Goldstein, Arthur W.
II. NACA TN 2388

NACA TN 2388

National Advisory Committee for Aeronautics. AXISYMMETRIC SUPERSONIC FLOW IN ROTATING IMPELLERS. Arthur W. Goldstein. June 1951. 36p. diagrs. (NACA TN 2388)

General equations are developed for isentropic, frictionless, axisymmetric compressible flow in rotating impellers with blade forces eliminated in favor of the blade-surface function. The characteristic equations for supersonic flow are developed and a computing technique is utilized to find the effect of variations of design parameters on internal flow and work-input distribution.

Copies obtainable from NACA, Washington

1. Flow, Supersonic (1.1.2.3)
2. Compressor Flow Theory and Experiment (3.6.1)
3. Compressors - Mixed Flow (3.6.1.3)

I. Goldstein, Arthur W.
II. NACA TN 2388